Atmos. Chem. Phys. Discuss., 15, 30269–30320, 2015
www.atmos-chem-phys-discuss.net/15/30269/2015/
doi:10.5194/acpd-15-30269-2015

Atmospheric Chemistry and Physics Discussions

Theoretical investigation of mixing in warm clouds – Part 2: Homogeneous mixing

M. Pinsky[1], **A. Khain**[1], **A. Korolev**[2], **and L. Magaritz-Ronen**[1]

[1]Department of Atmospheric Sciences, The Hebrew University of Jerusalem, Jerusalem, Israel
[2]Environment Canada, Cloud Physics and Severe Weather Section, Toronto, Canada

Received: 26 August 2015 – Accepted: 5 October 2015 – Published: 4 November 2015

Correspondence to: A. Khain (alexander.khain@mail.huji.ac.il)

Published by Copernicus Publications on behalf of the European Geosciences Union.

Abstract

The evolution of monodisperse and polydisperse droplet size distributions (DSDs) during homogeneous mixing is analyzed. Time-dependent universal analytical relations of supersaturation and liquid water content, which depend on a sole non-dimensional parameter, are obtained for a monodisperse DSD. The evolution of moments and moment-relation functions in the course of the homogeneous evaporation of polydisperse DSDs is analyzed using a parcel model.

It is shown that the classic conceptual scheme, according to which homogeneous mixing leads to a decrease in the droplet mass under constant droplet concentration, is valid only in cases of monodisperse or initially very narrow polydisperse DSDs. In cases of wide polydisperse DSDs, mixing and successive evaporation lead to a decrease of both mass and concentration such that the characteristic droplet sizes remain nearly constant. As this feature is typically associated with inhomogeneous mixing, we conclude that in cases of an initially wide DSD at cloud top, homogeneous mixing is nearly indistinguishable from inhomogeneous mixing.

1 Introduction

The process of mixing consists in smoothening of spatial gradients of inhomogeneities, such as temperature, water vapor, aerosol concentration, etc. In the cloudy environment mixing primarily occurs through turbulent and molecular diffusion (Monin and Yaglom, 1975). Thus, at the inertial subrange turbulence facilitates engulfing and mutual penetration of neighboring air volumes. During turbulent mixing, the shapes of mixing air volumes change, forming structures consisting of elongated and narrowed filaments. Turbulent mixing leads to the formation of inhomogeneous, fractal-like structures down to the Kolmogorov microscale. The molecular diffusion at the Kolmogorov microscale covers the gaps between the filaments, resulting in a total homogenization

ACPD
15, 30269–30320, 2015

of the mixing volumes (Kerstein, 1988, 1991). These processes have been described well by Monin and Yaglom (1975), see also Dimotakis (2005).

In cloud physics, different processes, namely entrainment, detrainment (de Rooy et al., 2013), isobaric mixing (Korolev and Isaac, 2000), homogeneous mixing and inhomogeneous mixing are referred to as *mixing* (Burner and Brenguier, 2006; Devenish et al., 2012; Kumar et al., 2013). Much scholarly attention has been paid on how mixing with entrained out-of-cloud dry air affects the formation of the droplet size distribution (DSD). Turbulent mixing at cloud edges and cloud tops accompanied by phase transitions has been the focus of numerous studies, beginning with the pioneering work of Baker and Latham (1979), Baker et al. (1980) and Blyth et al. (1980). In a laboratory experiments by Latham and Reed (1977) showed that some droplets completely evaporate while others remain unchanged after mixing with sub-saturated air. This finding gave rise to the concept of two types of turbulent mixing: homogeneous and inhomogeneous. It has been hypothesized that inhomogeneous mixing may lead to formation of superadiabatic-sized droplets, triggering the emergence of first raindrops. The classical concepts of homogeneous and inhomogeneous mixing are analyzed by Korolev et al. (2015, hereafter Pt1) in detail.

Figure 1 presents a conceptual scheme of homogeneous mixing between saturated cloudy volume V_1 containing droplets and sub-saturated droplet free volume V_2 (Fig. 1a). In the frame of the homogeneous mixing concept the air within the volumes mixes at the rate much faster than the characteristic rate of the droplet evaporation. So the temperature and humidity (and, therefore, the relative humidity and supersaturation) fields rapidly homogenize throughout the entire volume and all droplets will experience the same supersaturation (Fig. 1b). At the end of the first stage stage, the droplet concentration decreases due to dilution down to $N_0 = N_1 \frac{V_1}{V_1+V_2}$, where N_1 is the initial droplet concentration in the cloud volume. At the second stage (Fig. 1c) droplets responding on the environmental changes of supersaturation and temperature through their evaporation. There are two possible scenarios for the droplet response during the second stage. First, if the mixed air is too dry, than the droplets completely evaporate.

ACPD
15, 30269–30320, 2015

During the second scenario they will continue evaporating until they saturate the environment (see Pt1). As a result the size of all droplets decreases, while the droplet concentration N_0 remains unchanged (Fig. 1c).

In contrast to homogeneous mixing, the rate of homogenization during *extreme inhomogeneous* mixing is relatively low. According to the concept of extreme inhomogeneous mixing some droplets are transported by the turbulent eddies into the dry environment and experience complete evaporation, whereas other droplets remain unchanged. As in the case of homogeneous mixing the process of droplet evaporation continues until the initially droplet-free volume is saturated or all droplets evaporate. According to the classical concept, during extreme inhomogeneous mixing the shape of DSD is conserved, however the total droplet concentration decreases (see review by Devenish et al., 2012, Pt1).

Beginning with the work of Warner (1969) and Baker and Latham (1979) numerous observational and numerical studies investigating the effects of entrainment and mixing on DSD have been carried out (Devenish et al., 2012). Most of the theoretical studies were focused on the final state of mixing. If the droplet concentration decreased without changing the characteristic droplet size, then such mixing is considered to be extremely inhomogeneous. In contrast, if at the final stage characteristic droplet size but the droplet concentration remained unchanged, then such mixing was interpreted as homogeneous.

In this study, we analyze the time evolution of the DSD during the process of homogeneous mixing in cases of monodisperse and polydisperse initial DSDs. The analysis is based on new equations and the methodology used in studies by Pinsky et al. (2013, 2014).

It is anticipated that homogeneous and in-homogeneous mixing are spatial scale dependent processes. The characteristic spatial scale of homogeneous mixing can be estimated by comparing the characteristic times of two processes leading to thermodynamic equilibrium inside the resulting volume and the characteristic rate of spatial mixing. Baker and Latham (1982) were the first to describe mixing as a combination

ACPD
15, 30269–30320, 2015

of turbulent diffusion and droplet evaporation. The first process is mechanical mixing (diffusion), which is governed by turbulence. The turbulent mixing leads to the homogenization of temperature, humidity (and, thus, of supersaturation) and droplet concentration fields within the volume $V = V_1 + V_2$. The second process is the droplet evaporation, which leads to thermodynamical equilibrium of the environment.

Each of the two processes has its own characteristic time scale. The homogenization time τ_{mix} of an entrained volume with linear scale L_{mix} can be evaluated from the relationship (Monin and Yaglom, 1975)

$$\tau_{mix} = \varepsilon^{-1/3} L_{mix}^{2/3} \quad (1)$$

where ε is the turbulent kinetic energy dissipation rate. The characteristic time of molecular mixing at the Kolmogorov microscale is short enough to be neglected, unlike the turbulent mixing time determined by Eq. (1). The estimation Eq. (1) suggests that the size of the volume falls within an inertial interval of turbulence. Therefore, after the time of τ_{mix}, volume with a linear scale of about L_{mix} will be mechanically homogenized and all droplets in the volume will experience the same supersaturation.

The characteristic time of the second process, known as the *phase relaxation time*, τ_{pr} (Mazin, 1968; Korolev and Mazin, 2003), determines the rate of change of the supersaturation field

$$\tau_{pr} = (4\pi D \bar{r} N)^{-1}, \quad (2)$$

where $N = N_0$ is the concentration of droplets in the resulting volume, $\bar{r}$ is the mean radius of droplets and D is the diffusivity of water vapor molecules. The spatial scale at which the mixing time is equal to the phase relaxation time is called a phase relaxation scale L_{pr} (Mazin, 1968). This scale can be calculated from Eqs. (1) and (2) as

$$L_{pr} = \varepsilon^{1/2} \tau_{pr}^{3/2} \approx \varepsilon^{1/2} (4\pi D \bar{r} N)^{-3/2} \quad (3)$$

Therefore, after time τ_{pr} volume with a linear scale of about L_{pr} will be saturated because of droplet evaporation.

ACPD
15, 30269–30320, 2015

The value of the Damköhler number is used to determine the type of mixing (Lehmann et al., 2009)

$$Da = \frac{\tau_{mix}}{\tau_{pr}} = \frac{4\pi D\bar{r} N L_{mix}^{2/3}}{\varepsilon^{1/3}} \quad (4)$$

The case with $\tau_{mix} \ll \tau_{pr}$ or $Da \ll 1$ corresponds to extreme homogeneous mixing, i.e. mechanical homogenization due to turbulent mixing occurs much faster than does droplet evaporation. The case $Da \gg 1$ corresponds to extreme inhomogeneous mixing. It is reasonable to consider the value $Da = 1$ as a boundary separating two types of mixing. This condition is equivalent to the condition

$$L_{mix} = L_{pr} \approx \varepsilon^{1/2}(4\pi D\bar{r} N)^{-3/2} \quad (5)$$

Expression (5) determines the maximum spatial scale when mixing can be considered as homogeneous. The evaluations of the spatial scales under conditions typical of different cloud types are presented in Table 1. One can see that the characteristic volume size in which mixing can be considered as homogeneous ranges from 0.2 to 0.6 m. At larger scales, supersaturation within the total air volume is non-uniform and droplets experience different supersaturations, so the rates of evaporation within the volume may vary. In this case, the mixing should be considered as inhomogeneous. In the majority of cloud-resolving model applications, mixing is considered as homogeneous at substantially larger sub-grid scales. The problem of turbulent mixing representation in numerical cloud models is discussed in Sect. 5.

2 Thermodynamic characteristics of the resulting volume at the end of the first stage

The first stage of the process of homogeneous mixing is considered as an isobaric process that is not accompanied by phase transitions (Korolev and Isaac, 2000). Let

ACPD
15, 30269–30320, 2015

us consider the mixing of cloud volume with mass m_1, supersaturation $S_1 = 0$ and temperature T_1 and a non-cloudy volume with mass m_2, supersaturation $S_2 < 0$ and temperature T_2. The cloud volume also contains droplets with concentration N_1 and liquid water mixing ratio q_{w1} (see Fig. 1). For simplicity's sake, we assume that the mass of both parcels is equal to one. If the μ fraction of the mass from the cloud volume mixes with the $(1-\mu)$ fraction of the mass from the dry volume, then the air mass in the resulting volume will be equal to $m_1\mu + (1-\mu)m_2 = 1$. Isobaric mixing leads to an approximate linear dependence of droplet concentration, q_{w0} on μ.

After the instant homogenization of two volumes with ratio of mixing μ, the intermediate temperature T_0, droplet concentration N_0, and liquid mixing ratio q_0 will be

$$N_0 = N_1\mu; \quad q_{w0} = q_{w1}\mu; \quad T_0 = T_1\mu + T_2(1-\mu) \tag{6a}$$

In cases when the temperature difference $|T_1 - T_2|$ does not exceed few degrees, the intermediate supersaturation S_0 can be well approximated by a linear dependence vs. μ

$$S_0 = S_2(1-\mu) \tag{6b}$$

Figure 2 shows, that in case $|T_1 - T_2| < 2\,^{\circ}\mathrm{C}$ the deviations of supersaturation from linear dependence Eq. (6b) are small enough that and in the frame of this study they can be neglected. In cases where the temperature of the dry volume is substantially lower than the temperature of the cloud volume (such a situation typically obtains at the upper boundary of stratiform clouds in a zone of temperature inversion) the dependence of the resulting supersaturation on parameter μ becomes non-linear (see Fig. 2). The values of N_0, q_{w0}, T_0, and S_0 determine the initial conditions for the second stage of the homogeneous mixing process. This is essentially the homogeneous evaporation of droplets, which leads to a thermodynamic equilibrium between water vapor and liquid water.

ACPD
15, 30269–30320, 2015

3 Analysis of homogeneous droplet evaporation in the monodisperse case

3.1 Basic assumption and equations

The intermediate values N_0, q_{w0}, T_0, and S_0 constitute the initial conditions for the second stage of the homogeneous mixing process. The second stage of the mixing consists in homogeneous evaporation of droplets, which leads to a thermodynamic equilibrium between water vapor and liquid water.

The evolution of the DSD during the second stage will considered under the following assumptions: (a) the processes inside the volume are adiabatic; (b) the droplet size distribution is monodisperse; (c) the vertical velocity of the volume $u_z = 0$; (d) the sedimentation of droplets is neglected and their concentration remains constant.

The liquid water mixing ratio can be expressed as

$$q_w(t) = \frac{4\pi\rho_w}{3\rho_a} N r^3(t) \tag{7}$$

where $r(t)$ is the radius of droplets and N is the droplet number concentration. Closed equations describing the condensation/evaporation process in moving adiabatic air volume were obtained in a study by Pinsky et al. (2013). The unmovable adiabatic volume evaporation process is described by the equation for supersaturation found in Korolev and Mazin (2003)

$$\frac{1}{S+1}\frac{dS}{dt} = -A_2\frac{dq_w}{dt} \tag{8}$$

and the simplified equation of droplet evaporation (Pruppacher and Klett, 2007), in which the curvature term and the chemical composition term are omitted.

$$r\frac{dr}{dt} = \frac{S}{F} \tag{9}$$

ACPD
15, 30269–30320, 2015

where S is the supersaturation over a flat water surface. Equation (9) is valid with high accuracy for cloud droplets. We do not consider in this study the formation of haze particles resulting from evaporation. This allows us to neglect the curvature and chemical terms in the evaporation equation. Coefficients A_2 and F in Eqs. (8) and (9) are slightly dependent on air temperature and pressure

$$A_2 = \frac{1}{q_v} + \frac{L_w^2}{c_p R_v T^2} \tag{10}$$

$$F = \frac{\rho_w L_w^2}{k_a R_v T^2} + \frac{\rho_w R_v T}{e_w(T) D} \tag{11}$$

The physical meaning and units of other variables are given in Table A1. In this section we assume that coefficients A_2 and F do not change in the course of droplet evaporation.

3.2 Time evolution of supersaturation and LWC

In the following analysis, we use different forms of closed differential equations for the liquid water mixing ratio q_w and S. The corresponding equations are derived in Appendix B.

$$\frac{dq_w}{dt} = B N_0^{2/3} \left[(S_0 + 1) \exp\{-A_2 (q_w - q_{w0})\} - 1 \right] q_w^{1/3} \tag{12}$$

$$\frac{1}{S+1} \frac{dS}{dt} = -A_2 B N^{2/3} S \left(q_{w0} - \frac{1}{A_2} \ln \frac{S+1}{S_0+1} \right)^{1/3} \tag{13}$$

where

$$B = \frac{3}{F} \left(\frac{4\pi\rho_w}{3\rho_a} \right)^{2/3} = \text{const} \tag{14}$$

ACPD
15, 30269–30320, 2015

The solutions to these equations depend on the values of N_0, q_{w0}, T_0, and S_0 resulting from the first stage of mixing. Equations (12) and (13) are rigidly connected by the following equation directly following from Eq. (8):

$$\ln[S(t)+1] = -A_2 q_w(t) + C \tag{15}$$

where $C = \ln[S_0 + 1] + A_2 q_{w0}$ is determined by the initial conditions at $t = 0$.

In this study $S(t) \le 0$. In this case it is also convenient to use relative humidity RH and saturation deficit SD to characterize the thermodynamic state of the air volume. Both quantities are easily related to $S(t)$: $\mathrm{SD}(t) = -S(t)$, $\mathrm{RH}(t) = 1 + S(t)$. Figure 3 demonstrates dependencies $S(t)$ and $q_w(t)$, calculated under an initial relative humidity RH_0 that is varied from 72 to 91.6 % and an initial LWC of 0.6 g m^{-3}. RH_0 corresponds to the relative humidity in dry volume RH_2 that ranges from 43 to 83 % at $\mu = 0.5$. The results of the solutions of Eqs. (14) and (15) were compared with those obtained using a parcel model (Korolev, 1995) in which the process of evaporation was described using equations with temperature-dependent parameters. Excellent agreement is seen between the results obtained using Eqs. (12) and (13) and the results obtained using the parcel model. This agreement can be attributed to the fact that temperature changes that occurred in the course of mixing were relatively small, validating the assumption about the constancy of A_2 and F.

As seen from Fig. 3 the final equilibrium state may be reached within several seconds. Figure 3 shows two possible final states: (a) complete droplet evaporation, which is reached at different times depending on the initial S_0, and (b) partial droplet evaporation at $\mathrm{RH}_0 > 82$ %. In this case, the final value of supersaturation is equal to zero.

3.3 Universal dependencies of supersaturation and LWC on time

In order to simplify the following analysis we introduce the following non-dimensional parameters: normalized liquid water mixing ratio $\widetilde{q} = \frac{q}{q_{w0}}$, normalized supersaturation $\widetilde{S} = \frac{S}{A_2 q_{w0}}$, and non-dimensional time $t = t/\tau_0$, where $\tau_0 = (BA_2 N_0^{2/3} q_{w0}^{1/3})^{-1}$ is the time

ACPD
15, 30269–30320, 2015

scale. Then the set of non-dimensional equations describing changes of supersaturation and liquid mixing ratio can be written as (Appendix B)

$$\widetilde{S}(\widetilde{t}) = -\widetilde{q}(\widetilde{t}) + \gamma \tag{16}$$

$$\frac{\mathrm{d}\widetilde{q}}{\mathrm{d}\widetilde{t}} = \widetilde{q}^{1/3}(\gamma - \widetilde{q}) \tag{17}$$

$$\frac{\mathrm{d}\widetilde{S}}{\mathrm{d}\widetilde{t}} = -(\gamma - \widetilde{S})^{1/3}\widetilde{S} \tag{18}$$

where

$$\gamma = 1 + \frac{S_0}{A_2 q_{\mathrm{w0}}} \tag{19}$$

is the dimensionless parameter, which depends on initial supersaturation S_0 and initial liquid water mixing ratio q_{w0}. This parameter can be either positive or negative. Equations (16)–(18) are valid if the condition $|S_0| \ll 1$ is fulfilled, i.e. when the value of supersaturation S is neglected as compared with 1 in the factor $(S+1)^{-1}$ on the left-hand side of Eq. (8). Equation (17) should be solved with the initial condition $\widetilde{q}(0) = 1$, and Eq. (18) should be solved with the initial condition $\widetilde{S}(0) = \frac{S_0}{A_2 q_{\mathrm{w0}}} < 0$. Therefore, solutions of both equations depend on the sole parameterγ. Note, that Eqs. (17) and (18) are rigidly connected by balance equation Eq. (16).

Defining $x(\widetilde{t}) = (\widetilde{q}(\widetilde{t}))^{1/3}$ and $\chi = |\gamma|^{1/3} sgn(\gamma)$, the solution of Eq. (17) with initial condition $x(0) = 1$ is

$$2\chi\widetilde{t} = \ln\left[\frac{(1-\chi)^2}{(x-\chi)^2}\frac{x^2+\chi x+\chi^2}{1+\chi+\chi^2}\right] + 2\sqrt{3}\left[a\tan\frac{2\sqrt{3}\chi(1-x)}{3\chi^2+(2+\chi)(2x+\chi)}\right] \tag{20}$$

The solution for normalized supersaturation can be obtained from Eq. (20) and balanced Eq. (16)

$$\widetilde{S}(\widetilde{t}) = -\widetilde{q}(\widetilde{t}) + \gamma = -x^3(\widetilde{t}) + \chi^3 \tag{21}$$

ACPD
15, 30269–30320, 2015

Figure 4 demonstrates the behavior of $\widetilde{S}(\widetilde{t})$ and $\widetilde{q}(\widetilde{t})$, calculated for different γ. In these calculations the initial supersaturation $S_0 > -10\,\%$ (i.e. $RH_0 > 90\,\%$). As seen from Fig. 4 the analytical solution is quite close to the modeled one. The deviation increases with an increase in parameter γ. At $\gamma = -0.5$, the error in the final RH is about 15 %. The initial RH_0 in this case is about 90 %. Note that RH_0 is the intermediate relative humidity in the volume V after the first stage of mixing. As mentioned above, RH_0 may be substantially higher than that found in the initially dry volume RH_2. These considerations indicate that analytical Eqs. (17) and (18) may be applicable within a wide range of RH_2 down to quite low values. Note that in situ measurements (Gerber et al., 2008) and remote measurements of aerosol humidification (Knight and Miller, 1998; Bar-Or et al., 2012) indicate the existence of zones of high RH in the cloud environment along cloud edges. These observations indicate applicability of the assumptions $|S_0| \ll 1$ to real cloud conditions.

The amplitude of the deviation of the analytical solution from the modeled result decreases with the decrease of γ, and it is related to the neglecting of the term $(S+1)$ in the left-hand side of Eq. (8).

There are two types of solutions determined by parameter χ (or parameter γ), separated by value $\chi = 0$. These types of solutions are seen in Figs. 3 and 4. Condition $\chi > 0$ corresponds to solutions demonstrating asymptotic behaviors at $\widetilde{t} \to \infty$: $\widetilde{q} \to \gamma$ and $\widetilde{S} \to 0$. This solution means that not all droplets evaporate in a mixed volume. Condition $\chi < 0$ corresponds to situations when all droplets fully evaporate. Condition $\chi = 0$ corresponds to a boundary situation, when all droplets evaporate, increasing relative humidity up to 100 %.

In the case of $\chi = 0$ the analytical solution is:

$$x = \frac{3}{\widetilde{t}+3}; \quad \widetilde{q}(\widetilde{t}) = \left(\frac{3}{\widetilde{t}+3}\right)^3; \quad \widetilde{S}(t) = -\left(\frac{3}{\widetilde{t}+3}\right)^3 \tag{22}$$

Both LWC and supersaturation tend to zero when $\widetilde{t} \to \infty$.

ACPD
15, 30269–30320, 2015

At $\chi < 0$ the evaporation process is limited in time (Figs. 3 and 4). Normalized on τ_0 evaporation time t_e depends on parameterχ only. This dependence can be obtained from Eq. (20) in which $x = 0$:

$$t_e = \frac{1}{2\chi} \ln \frac{(1-\chi)^2}{1+\chi+\chi^2} + \frac{\sqrt{3}}{\chi} a\tan \frac{\sqrt{3}}{2\chi+1} \tag{23}$$

Here the time is counted by the number of relaxation time scales. In the case of $\chi > -1/2$, one should use the values $a\tan\frac{\sqrt{3}}{2\chi+1} - \pi$ in Eq. (23) instead of $a\tan\frac{\sqrt{3}}{2\chi+1}$. t_e is also the time that is needed for supersaturation to reach its maximal value (Figs. 3a and 4a). This value is calculated from Eqs. (16) and (6)

$$\widetilde{S}_{\max} = \gamma = \chi^3 = 1 + \frac{S_0}{A_2 q_{w0}} \approx 1 + \frac{S_2}{A_2 q_{w1}} \frac{1-\mu}{\mu} = 1 + R\frac{1-\mu}{\mu} \tag{24}$$

where $R = \frac{S_2}{A_2 q_{w1}}$ is a dimensionless parameter.

The dependence $t_e(\chi)$ is shown in Fig. 5.

One can see that at large sub-saturations ($\chi < -0.4$) all droplets evaporate within the span of a few relaxation times, and the analytical results agree well with the model (benchmark) results. At a high initial RH, droplet evaporation increases humidity to nearly saturation value, so the process of evaporation becomes extremely slow. In this case, simplified analytical formulas overestimate the evaporation time.

In the case of $\chi > 0$, droplets partially evaporate, LWC reaches a minimal value and thermodynamic equilibrium reaches when $S \to 0$. Minimal normalized equilibrium LWC can be found from Eqs. (21) and (6)

$$\widetilde{q}_{\min} = \gamma = \chi^3 = 1 + R\frac{1-\mu}{\mu} \tag{25}$$

Equation (25) is similar to Eqs. (8) and (9) in Pt1.

ACPD
15, 30269–30320, 2015

Dependences of $\widetilde{S}_{max}$ and $\widetilde{q}_{min}$ on cloud air fraction, calculated using Eqs. (24) and (25) are shown in Fig. 6. The diagrams shown in Fig. 6 actually describe the final results of homogeneous evaporation under different initial conditions. The advantage of these diagrams is that the dependencies are plotted as a function of non-dimensional parameter R describing the ratio of S_2 in the initially dry air and the reserve of liquid water for evaporation. Thus, the diagrams are universal. Panel (a) shows the natural result that the higher the cloudy fraction of air parcels involved in mixing, the lower the saturation deficit, i.e. the higher is the final RH. At small R saturation is reached at a low cloud air fraction.

The obtained equations allow prediction of the results of homogeneous mixing both for the cases of partial or complete evaporation of droplets. Some estimations are given in Table 2. One can see from Table 2 that that at low temperatures comparatively small values of liquid water content in cloudy volume are necessary to make environment volume cloudy by mixing even if RH of the environment volume is as low as 50 %. It is because saturation ratio at low temperatures is low and only small amount of liquid should be evaporated to make the volume saturated. The mixing volume can become non-cloudy only if the initial environment volume is substantially larger than that of cloudy one (see Pt1 for detail).

The diagram in Fig. 6b allows for a calculation of the final liquid water content remaining in the entire volume after saturation reaches 100 %. This diagram also shows that at each value of μ there is a certain value of R, when full evaporation takes place before RH reaches 100 %. The remaining LWC increases with a decrease of μ and increases in R, as shown by the arrow.

The natural time scale of the problem (evaporation and, therefore, homogeneous mixing) was determined as $\tau_0 = (BA_2N_0^{2/3}q_{w0}^{1/3})^{-1}$. This value is inversely proportional to N_0r_0 and actually coincides with the initial phase relaxation time τ_{pr}. The equality of the characteristic time scales of variation of supersaturation and liquid water content directly follows from the Eq. (15). Indeed, in the case of $|S| \ll 1$ the equation can

ACPD
15, 30269–30320, 2015

be rewritten as $S(t) = -A_2 q_w(t) + C$ that relates linearly the supersaturation and liquid water mixing ratio.

Figures 3 and 4 show that the characteristic time of homogeneous evaporation is close to the phase relaxation time. During this time, significant fraction of the available droplet mass evaporates, and supersaturation increases accordingly. It should be emphasized that this time is not the time of total drop evaporation or the time of reaching saturation (if evaporation terminates). Time of complete evaporation or time of evaporation termination can be dozens of times more that phase relaxation time τ_0 (see also Pt1, Fig. 15).

4 Analysis of homogeneous droplet evaporation in the polydisperse case

4.1 DSD evolution in the course of droplet evaporation

To analyse polydisperse DSD evolution during droplet evaporation at the second stage of homogeneous mixing, we use the equations for diffusional growth Eq. (9) and supersaturation Eq. (8) that are used in the case of a monodisperse DSD. The solution of Eq. (9) can be written in the form

$$r^2(t) = r_0^2 - Q(t) \tag{26}$$

where the non-negative function $Q(t) \geq 0$ is proportional to the supersaturation integral

$$Q(t) = -\frac{2}{F}\int_0^t S(t')\mathrm{d}t' \geq 0 \tag{27}$$

This function characterizes decrease in square of droplet radii which is the same for droplets of different sizes. At $t = 0$, $Q(0) = 0$. Let $f_0(r_0)$ be an initial DSD just after the

ACPD
15, 30269–30320, 2015

first stage of homogeneous mixing. This distribution obeys the normalization condition

$$N_0 = \int_0^\infty f_0(r_0)\mathrm{d}r_0 \tag{28}$$

where N_0 is the initial droplet number concentration after first stage of mixing. Using the inverse transformation $r_0 = \sqrt{r^2 + Q(t)}$ alongside condition $r \geq 0$ and the relation between distribution functions $f(r,t) = f_0(r_0)\frac{\mathrm{d}r_0}{\mathrm{d}r}$ we get

$$f(r,t) = \begin{cases} \frac{r}{\sqrt{r^2+Q(t)}} f_0\left(\sqrt{r^2+Q(t)}\right), & r \geq 0 \\ 0, & r < 0 \end{cases} \tag{29}$$

Equation (29) shows that the time changes of DSD and its moments depend on the initial DSD at $t = 0$, $f_0(r_0)$, and on the time-dependent function $Q(t) \geq 0$.

To illustrate the evolution of the DSD using Eq. (29), we assume that the initial distribution just after the first stage of mixing can be represented by a Gamma distribution:

$$f_0(r_0) = \frac{N_0}{\Gamma(\alpha)\beta}\left(\frac{r_0}{\beta}\right)^{\alpha-1}\exp\left(-\frac{r_0}{\beta}\right) \tag{30}$$

where N_0 is an intercept parameter, α is a shape parameter and β is a slope parameter of distribution. Different sets of parameters allow for approximations of both narrow and wide DSDs. The parameters of the initial Gamma distribution used in this study are presented in Table 3. Parameters are chosen so that the modal radii of DSDs and LWCs would be the same for both distributions.

Combining Eqs. (29) and (30), yields the equation for DSD evolution as a function of $Q(t)$

$$f(r,t) = \begin{cases} \frac{N_0}{\Gamma(\alpha)\beta^\alpha}(r^2+Q)^{\frac{\alpha}{2}-1} r \exp\left(-\frac{\sqrt{r^2+Q}}{\beta}\right), & r \geq 0 \\ 0, & r < 0 \end{cases} \tag{31}$$

ACPD
15, 30269–30320, 2015

This DSD Eq. (31) depends on four parameters, wherein the parameter $Q(t)$ increases with time according to Eq. (27). Examples of an initially narrow DSD evolution and an initially wide DSD evolution are shown in Fig. 7. All calculations were performed using a parcel model (Korolev, 1995).

There is a significant difference between evaporation of monodisperse and polydisperse size distributions. For the monodisperse case the droplet concentration remains unchanged until the final stage of evaporation when droplets become small and then all of them rapidly evaporate. At that point their concentration instantly drops to zero. However, for the case of polydisperse case the droplet concentration decreases simultaneously with the decrease of LWC. So the evaporation of the narrow size distribution is consistent with the concept of homogeneous mixing (Fig. 7a). However homogeneous evaporation of a wide DSD can be confused with inhomogeneous mixing.

4.2 Evolution of moments and related functions

Equation (29) also allows for the evaluation of droplet concentration, DSD moments and related functions. Droplet concentration corresponds to the zero moment of DSD and can be expressed as

$$N(t) = \int_0^\infty f(r,t)\mathrm{d}r = \int_0^\infty \frac{r}{\sqrt{r^2+Q(t)}} f_0\left(\sqrt{r^2+Q(t)}\right)\mathrm{d}r = \int_{\sqrt{Q(t)}}^\infty f_0(r_0)\mathrm{d}r_0 \tag{32}$$

Since function $Q(t)$ monotonically increases with the time, right integral in Eq. (32) decreases that indicates a decrease in droplet concentration with the time. If the initial distribution of droplets is described by a Gamma distribution, the decrease of droplet

ACPD
15, 30269–30320, 2015

concentration with the time is evaluated from Eqs. (30) and (32)

$$N(t) = \int_{\sqrt{Q(t)}}^{\infty} f_0(r_0,t)\mathrm{d}r_0 = \int_{\sqrt{Q(t)}}^{\infty} \frac{N_0}{\Gamma(\alpha)\beta}\left(\frac{r_0}{\beta}\right)^{\alpha-1}\exp\left(-\frac{r_0}{\beta}\right)\mathrm{d}r_0$$

$$= \frac{N_0}{\Gamma(\alpha)}\int_{\frac{\sqrt{Q(t)}}{\beta}}^{\infty} x^{\alpha-1}\exp(-x)\mathrm{d}x = N_0\frac{\Gamma(\alpha,\eta)}{\Gamma(\alpha)}.$$

$$N(t) = \frac{N_0}{\Gamma(\alpha)}\Gamma(\alpha,\eta(t)) \tag{33}$$

where

$$\eta(t) = \frac{\sqrt{Q(t)}}{\beta} \tag{34}$$

is a non-dimensional function of the time and $\Gamma(\alpha,\eta(t))$ is an upper incomplete Gamma function (Korn and Korn, 2000). It is seen from Eqs. (32) and (33) that $N(t) \le N_0$. The dependencies of normalized droplet concentration $\frac{N(t)}{N_0}$ on time for initially narrow and wide DSDs are shown in Fig. 8.

Figure 8 shows that in the case of an initially narrow DSD, droplet concentration does not change during the first 20 s when $RH_0 = 91.6\,\%$ because the DSD does not shift strongly enough toward smaller droplet radii. At lower initial supersaturations, droplet concentration decreases with time in the case of a narrow DSD. This decrease can take place very quickly, and may last several seconds only. The red line separates two different scenarios of evaporation. The cases above the red line correspond to partial evaporation and reaching the saturation state, whereas the cases below the red line result in complete evaporation of droplets and the environment remains undersaturated. In the second case, the remaining droplet concentration is negligibly small, but it is not

ACPD
15, 30269–30320, 2015

exactly equal to zero because of the existence of several very large drops in the tail of the Gamma distribution.

With regard to an initially wide DSD, droplet concentration decreases at any initial subsaturation because the wide DSD contains small droplets that start evaporating at any subsaturation value. In the particular example, the drop relaxation time is smaller in the case of a wide DSD, so the droplet concentration decreases slower than in the case of a narrow DSD. Droplet concentration decreases substantially during a few tens of seconds, but does not drop to zero due to a significant concentration of large droplets in the wide DSD. The equilibrium state is not reached in 20 s.

Figure 8 also demonstrates excellent agreement between the analytical calculations from Eq. (33) and those obtained using the parcel model.

A normalized moment of the kth order is evaluated as

$$\overline{r^k(t)} = \frac{1}{N(t)} \int_0^\infty r^k f(r,t) \mathrm{d}r = \frac{1}{N(t)} \int_0^\infty \frac{r^{k+1}}{\sqrt{r^2+Q(t)}} f_0\left(\sqrt{r^2+Q(t)}\right) \mathrm{d}r$$

$$= \frac{1}{N(t)} \int_{\sqrt{Q(t)}}^\infty \left(r_0^2 - Q(t)\right)^{k/2} f_0(r_0) \mathrm{d}r_0$$

$$\overline{r^k(t)} = \frac{\int_{\sqrt{Q(t)}}^\infty \left(r_0^2 - Q(t)\right)^{k/2} f_0(r_0) \mathrm{d}r_0}{\int_{\sqrt{Q(t)}}^\infty f_0(r_0) \mathrm{d}r_0} \quad (35)$$

ACPD
15, 30269–30320, 2015

In the case where the initial distribution is given by Gamma distribution (Eq. 30), Eq. (35) leads to the following equation

$$\overline{r^k}(t) = \frac{\beta^k}{\Gamma(\alpha, \eta(t))} \int_{\eta(t)}^{\infty} (x^2 - \eta^2(t))^{k/2} (x)^{\alpha-1} \exp(-x) \mathrm{d}x \tag{36}$$

Even moments can be represented using incomplete Gamma functions.

Figures 9 and 10 show the time dependencies of quantities typically used for characterizing the DSD shape, namely the mean radius $\overline{r}(t)$ (panel a), effective radius $r_{\mathrm{eff}}(t) = \frac{\overline{r^3}(t)}{\overline{r^2}(t)}$ (panel b), RMS width of DSD $\sigma(t) = \sqrt{\overline{r^2}(t) - \overline{r}^2(t)}$ (panel c) and dispersion coefficient $\delta(t) = \frac{\sigma(t)}{\overline{r}(t)}$ (panel d). The dependencies corresponding to an initially narrow DSD are shown in Fig. 9 and those corresponding to an initially wide DSD are shown in Fig. 10.

In the case of an initially narrow DSD, the mean radius and effective radius decrease with time in agreement with the widely accepted concept of homogeneous mixing. The formation of plateaus in the mean and effective radii and droplet dispersion over long time periods is caused by the existence of droplets in the tail of DSD distributions. The concentration of such droplets is negligibly small, but their evaporation takes a significant amount of time.

In the case of an initially wide DSD (Fig. 7b), the complete evaporation of the smallest droplets starts at the very beginning of the second stage of mixing. This evaporation process leads to an increase in the mean and effective radius (the mean radius changes non-monotonically). An increase in the value of the effective radius contradicts the concept of homogeneous mixing, according to which the mean and effective radii do not change. However, the explanation for this growth is simple: subsaturation in the case of an initially wide DSD leads to a significant decrease in the concentration of small droplets, while the changes in LWC, whose value is determined by larger droplets, do not occur as quickly.

ACPD
15, 30269–30320, 2015

The opposite behaviors of the effective radii (as well as the other characteristic drop sizes) in the cases of the narrow and wide DSDs illustrated in Figs. 9 and 10 suggest the existence of numerous DSDs in clouds with initial shapes at which the evaporation of droplets in the course of homogeneous mixing leads to a decrease in droplet concentration, but does not change significantly the effective radius. In these cases, the constancy of the effective radius under varying droplet concentrations does not allow to distinguish the mixing type. Even in the case of a narrow DSD, the decrease in the value of the effective radius does not exceed 20 % under an initial saturation deficit of 8.4 %.

In all cases, the evolution of DSDs and their parameters is determined by the competition between two effects. The first of these is partial droplet evaporation, which shifts the DSD toward smaller sizes and leads to a decrease in the mean and effective radii and an increase in the DSD width. The second effect is the complete evaporation of the smallest droplets, which leads to an increase in the mean and effective radii. The relative contribution of these two effects depends on the initial DSD width and the value of the mean radius. The best indicators of these two effects are the DSD width, σ and the DSD dispersion $\frac{\sigma}{r}$.

In the case of an initially narrow DSD and an initially low RH, the process of partial evaporation initially dominates and the DSD width first increases (Fig. 9c). This increase is caused by the appearance of smaller droplets. This effect is similar to the decrease in DSD width that occurs during diffusion growth. Then, when the complete droplet evaporation becomes the dominant factor, the DSD shifts significantly to small sizes and the DSD width decreases. In the case of an initially large RH, the complete droplet evaporation is not efficient, and continuous growth in the DSD width takes place. Since the mean radius decreases, the DSD dispersion tends to constant values at any initial RH. However, the largest DSD dispersion takes place at an initially low RH, when evaporation substantially decreases the mean droplet radius. As seen in Figs. 9d and 10d the initial DSD dispersion in the case of a narrow DSD is 0.1, while the initial dispersion in the case of a wide DSD is 0.5.

ACPD
15, 30269–30320, 2015

Figure 10c and d shows that in the case of an initially wide DSD, homogeneous evaporation leads to an increase in both DSD width and DSD dispersion. The increase in DSD width indicates that the formation of the smallest droplets by partial evaporation is the main mechanism of the DSD shape evolution in the case of wide DSDs. The DSD dispersion increases with time, and rapidly reaches quasi-stationary values of about 0.56. Note that these values are typical of real clouds.

4.3 Evolution of LWC and supersaturation

Using Eq. (35) decrease in liquid water mixing ratio is represented as follows

$$q_{\mathrm{w}}(t) = \frac{4\pi\rho_{\mathrm{w}}}{3\rho_{\mathrm{a}}} N(t)\overline{r^3(t)} = \frac{4\pi\rho_{\mathrm{w}}}{3\rho_{\mathrm{a}}} \int\limits_{\sqrt{Q(t)}}^{\infty} \left(r_0^2 - Q(t)\right)^{3/2} f_0(r_0)\mathrm{d}r_0 \tag{37}$$

If the initial DSD is approximated by a Gamma distribution, $q_{\mathrm{w}}(t)$ is represented as follows

$$q_{\mathrm{w}}(t)\frac{4\pi\rho_{\mathrm{w}}}{3\rho_{\mathrm{a}}} \int\limits_{\sqrt{Q(t)}}^{\infty} \left(r_0^2 - Q(t)\right)^{3/2} \frac{N_0}{\Gamma(\alpha)\beta}\left(\frac{r_0}{\beta}\right)^{\alpha-1} \exp\left(-\frac{r_0}{\beta}\right)\mathrm{d}r_0 =$$

$$\frac{4\pi\rho_{\mathrm{w}}}{3\rho_{\mathrm{a}}}\frac{N_0\beta^3}{\Gamma(\alpha)} \int\limits_{\eta(t)}^{\infty} (x^2 - \eta^2(t))^{3/2}(x)^{\alpha-1}\exp(-x)\mathrm{d}x$$

$$q_{\mathrm{w}}(t) = \frac{4\pi\rho_{\mathrm{w}}}{3\rho_{\mathrm{a}}}\frac{N_0\beta^3}{\Gamma(\alpha)} \int\limits_{\eta(t)}^{\infty} (x^2 - \eta^2(t))^{3/2}(x)^{\alpha-1}\exp(-x)\mathrm{d}x \tag{38}$$

ACPD
15, 30269–30320, 2015

Since at $t = 0$, $\eta = 0$ and the initial liquid water mixing ratio is equal to $q_{w0} = \frac{4\pi\rho_w}{3\rho_a} N_0 \beta^3 \frac{\Gamma(\alpha+3)}{\Gamma(\alpha)}$, the normalized liquid water mixing ratio is calculated as follows

$$\frac{q_w(t)}{q_{w0}} = \frac{1}{\Gamma(\alpha+3)} \int_{\eta(t)}^{\infty} (x^2 - \eta^2(t))^{3/2} (x)^{\alpha-1} \exp(-x) dx \quad (39)$$

Figure 11 shows the dependencies of LWC on the time for different initial RH_0 in the resulting volume. Figure 11a corresponds to an initially narrow DSD, while panel Fig. 11b corresponds to an initially wide DSD. One can see that in the case of an initially narrow DSD, the LWC rapidly decreases, either to zero (full evaporation) or to an equilibrium value as in the monodisperse case during a time period of the phase relaxation time (see Sect. 3 for comparison). In the case of an initially wide DSD, the LWC decreases slowly and monotonically. In general, the time dependencies, $q_w(t)$, in the case of a initially narrow DSDs are quite close to those in the case of monodisperse DSDs (Fig. 3b). The higher the initial RH, the smaller the change in the LWC.

To calculate the time dependencies of supersaturation, one can use full Eqs. (8) or (15) written in the form:

$$S(t) = (S_0 + 1) \exp\{-A_2[q_w(t) - q_{w0}]\} - 1 \quad (40)$$

In Eq. (40) S_0 and q_{w0} are the initial supersaturation and the liquid water mixing ratio, respectively, at $t = 0$. The corresponding time dependencies are shown in Fig. 12. The analytical results of Eq. (40) are compared with the exact solution of a parcel model. One can note good agreement between the analytical and the numerical (parcel model) results. The behavior of supersaturation in the case of a narrow DSD is similar to that of a monodisperse DSD (see Fig. 3a). As in Fig. 3a, the equilibrium non-zero values of subsaturation correspond to the complete droplet evaporation. In the case of a wide DSD, the saturation deficit monotonically decreases as a consequence of a monotonic decrease in the LWC (evaporation of droplets).

ACPD
15, 30269–30320, 2015

Figure 13 shows the dependencies of normalized LWC on normalized number concentrations of droplets calculated under different initial relative humidity RH_0 in the resulting volume. The dependencies are calculated for an initially narrow DSD (a) and an initially wide DSD (b). Each point on the curves corresponds to a certain time. Since the dependencies are plotted in non-dimensional coordinates, the time instance $t = 0$ corresponds to coordinates $(1, 1)$. The numbers along the curves denote the points corresponding to time instance $t = 20$ s. In the case of a lower RH_0 the curves reach lower values of LWC and droplet concentration.

In the case of an initially narrow DSD, one can see three separate zones. The first zone corresponds to a high RH_0 ($RH_0 > 90\,\%$). Within this zone, the droplet concentration does not decrease with a decrease in the LWC, which is in line with the conceptual scheme of homogeneous mixing (Fig. 1). This curve corresponds to the horizontal straight line in Fig. 8a. At lower relative humidity, the droplet concentration begins to decrease with a decrease in LWC, in line with Fig. 8a. When the LWC reaches small values, the dependence of the normalized LWC on the normalized droplet concentration becomes close to linear. In the case of an initially wide DSD (Fig. 13b), the dependence of the LWC on droplet concentration is close to linear at all values of RH_0 tested. Such linear dependence means that the mean volume radius varies only slightly during the evaporation process.

It is of interest that all curves plotted for different initial values RH_0 coincide. Such a coincidence can be explained by the fact that the DSDs used depend on four parameters: three parameters of the initial Gamma distribution and on $Q(t)$ (Eq. 31). The parameters of Gamma distributions are the same for every panel of Fig. 13. Parameter $Q(t)$ monotonically increases with time. At different RH_0, the values of $Q(t)$ reach the same values at different times. But when the values of $Q(t)$ are the same, the DSDs and all their moments are equal.

In summary, the case of a narrow DSD and a comparatively large initial relative humidity $RH_0 > 87\,\%$ demonstrates properties typically attributed to homogeneous mixing, when a decrease in both the LWC and the effective radius takes place at un-

ACPD
15, 30269–30320, 2015

changed droplet concentration (see Figs. 8a, 9b, 11a, and 13a). In contrast, in the case of an initially wide DSD, the evolution of the DSD and its moments is close to that typically attributed to inhomogeneous mixing, when the evaporation leads to a decrease in LWC and droplet concentration, but the effective radius remains unchanged. The shapes of the wide DSDs remain similar during the process of evaporation (Fig. 7b), which is considered usually as a characteristic feature of inhomogeneous mixing.

5 Application of the concept of homogeneous mixing in numerical modeling

The first question that arises with regard to the application of mixing algorithms to cloud models is: "What type of mixing do the models describe"? This question pertains to both the Euilerian models, which calculate microphysical variables on finite different grids (e.g., Benmoshe et al., 2012) and the Lagrangian–Euilerian models, where microphysical values are calculated within movable air parcels (e.g., Pinsky et al., 2008; Magaritz et al., 2009; Magaritz-Ronen et al., 2014). Mixing involves two steps at each model time-step. First, a calculation of turbulent flux divergence of thermodynamic and microphysical quantities between neighbouring parcels or grid points is performed by solving the equation of turbulent diffusion; second, the changes in microphysical values in the parcels or grid points are calculated using these flux divergences.

For time-steps and grid spacing typically used in these models, the changes caused by mixing during a single time-step are small and they do not entirely eliminate spatial gradients of microphysical variables between the mixing parcels (or neighbouring grid points). This stage represents inhomogeneous mixing at resolving scales. In contrast, the changes in the microphysical and thermodynamical variables inside each parcel (or grid points) are considered to be uniform at each time step, and therefore, the modelled mixing can be considered as homogeneous. So, in the numerical simulations, at model domain mixing is inhomogeneous, whereas inside each grid point at every time-step the mixing is homogeneous. Note that the mixing algorithms in models do not operate

ACPD
15, 30269–30320, 2015

with "final" equilibrium values (as assumed in the classical mixing concepts), but with current time-dependent values.

The estimations in Table 1 indicate that mixing should be considered as homogeneous at scales lower than ∼ 0.5 m. This means that to simulate homogeneous mixing explicitly the grid spacing (or parcel size) should be less that 0.5 m. In case such grid spacing is used, the separation between mixing types would be described explicitly. However, grid spacing (and parcel size) in most models is substantially larger than this value. The modern models separate mixing types at a substantially larger scale than that in Table 1. This brings up a questions: "What error is introduced when the spatial scale that separates mixing types in models is much larger than 0.5 m, and "Why are spectral microphysics models with a resolution of 40–50 m able to reproduce observed DSDs and their moments with high accuracy (Benmoshe et al., 2012; Khain et al., 2013, 2015; Magaritz-Ronen et al., 2014)?"

There are several factors that compensate errors in segregating type of mixing in cloud models and allow using grid scale $L > L_{pr}$ with little effect on DSD. The first factor is that mixing leads to the formation of homogeneous zones in clouds characterized by a spatial correlation radius of temperature, humidity and droplet concentration of about 150–250 m (Magaritz-Ronen et al., 2014). Numerical experiments (Magaritz-Ronen et al., 2014) with parcels of linear sizes of 20 and 40 m have shown that the results are not sensitive to the choice of parcel size if the parcel size is substantially smaller than the spatial radius of correlation. Therefore, type of mixing have a minor effect on the results of mixing at scales lower than the radius of correlation.

The second factor is that in many cases in-cloud mixing takes place at conditions close to saturation. At such a high humidity, results of homogeneous and inhomogeneous mixings become indistinguishable from one another. Indeed, the mixing diagrams in the case of a low saturation deficit do not allow for a separate type of mixing, since in this case the effective (or mean volume) radius does not change as a result of mixing (Burnet and Brenguier, 2006). The similarity of results for the two mixing types

ACPD
15, 30269–30320, 2015

is attributable to the fact that mixing in clouds is not accompanied by an appreciable phase transition.

Hill et al. (2009) explained the insensitivity of the evolution of stratocumulus clouds to the sub-grid mixing assumption by the fact that the rates of condensation/evaporation caused by resolved dynamics are two orders of magnitude greater than the condensation/evaporation rate caused by sub-grid processes. Changes in DSDs during turbulent mixing are caused by low intensity turbulent fluctuations of supersaturation, which are several orders of magnitude weaker than the corresponding processes at resolved scales.

The third factor that permits us to treat sub-grid mixing as homogeneous near cloud interfaces is that DSDs are polydisperse, which is opposite what is assumed in the conventional mixing considerations. In the present study it was shown that for a broad DSD, the changes of r_{eff} remain small during mixing. So, a relatively small partial evaporation of droplets provide sufficient amount of water vapor for saturation of the volume. In this case homogeneous mixing will become indistinguishable from inhomogeneous. The saturation of the volume may be facilitated by entrainment of water vapor from neighboring cloud volumes. The existence of high RH in the air volumes in the vicinity of cloud edges is reported and discussed by Gerber et al. (2008).

We believe that the obtained results justify the use of parcel models for the analysis of microphysical processes in cloud volumes ascending several hundred and even thousands of meters (Pruppacher and Klett, 1997; Korolev, 1995; Pinsky and Khain, 2002; Korolev and Isaac, 2003; Ghan et al., 2011; Pinsky et al., 2013). The linear scale of these parcels is certainly assumed to be on the order of several hundred meters (e.g., Ferrier et al., 1989; Anthes, 1982). The air in such volumes is assumed to be well mixed, i.e. all droplets experience the same supersaturation, thus fulfilling the definition of homogeneous mixing.

ACPD
15, 30269–30320, 2015

6 Conclusions

The present study is focused on the dynamics of transformation of DSD during the evaporation stage of homogeneous mixing.

1. Analytical equations are obtained for normalized supersaturation and normalized LWC on a cloud air fraction that describes the rate of evolution of the microphysics of mixing volume. These quantities turned out to be functions of one non-dimensional parameter $R = \frac{S_2}{A_2 q_{w1}}$. Such dependencies are universal, and allow for the calculation of the microphysical parameters of the final stages of mixing. In particular, universal dependencies are obtained for the calculation of the LWC required to saturate the total volume at different cloud fractions and the initial RH of the dry volume. It is shown that the major changes in the LWC take place during the time of the order of phase relaxation time, τ_{pr}. At the same time, the equilibrium state is reached after several τ_{pr}.

2. One of the most important outcomes of this work is demonstration of a big difference between evaporative behavior of narrow and broad DSD. It was shown that homogeneous evaporation of a broad DSD is accompanied by reduction of LWC and reduction of concentration due to evaporation of small droplets. Such behavior is qualitatively different from the conventional concept of homogeneous mixing and it may be mixed up evaporation of a population of droplets which occur during inhomogeneous mixing. It may lead to the fact that the cases of homogeneous mixing may be interpreted as inhomogeneous.

3. It is shown that the evolution of DSDs, and their moments in the case of polydisperse DSDs, can qualitatively differ from that which is predicted by homogeneous mixing. First, in the case of a polydisperse DSD, the concentration of droplets decreases due to evaporation. Since small droplets evaporate first, the changes to the effective radius are smaller than in the case of a monodisperse DSD. Evaporation in a comparatively wide DSD even leads to an increase in the effective

ACPD
15, 30269–30320, 2015

radius. These results show that homogeneous mixing may lead to a decrease in droplet concentration, but do not change the high DSD moments, including the effective radius. Such behavior is typically attributed to inhomogeneous mixing.

The last comment concerns very different roles of the polydispersity of DSD in the processes of mixing and in diffusion droplet growth in the ascending parcels. In the case of diffusion growth within an ascending adiabatic parcel, the supersaturation tends to zero with height, and the DSD width decreases with height as well. In this case, it is possible to reproduce height and time dependencies of supersaturation and LWC using an "equivalent" monodisperse DSD with the droplet concentration found in polydisperse DSDs (Pinsky et al., 2014). In contrast, the behaviour of the mixing process with polydisperse DSDs cannot be reproduced using monodisperse DSDs, with the possible exception of an initially extremely narrow DSD. (There is some similarity between Fig. 3 on the one hand and Figs. 11a and 12a). This result is related to two facts: (a) in the mixing process the absolute values of the initial supersaturation deficit can be much larger than supersaturations in the ascending adiabatic parcels; and (b) evaporation takes place during the mixing process, which leads to an increase in the DSD width; which is opposite to the diffusion growth process leads to a DSD narrowing.

Appendix A: List of symbols

The physical meaning and units of other variables are given in Table A1.

Appendix B: Derivation of closed equations for supersaturation and for liquid water mixing ratio in the monodisperse case

Let us consider motionless well-mixed adiabatic air volume having an initial supersaturation $S_0 < 0$ and an initial liquid water mixing ratio q_{w0}.

ACPD
15, 30269–30320, 2015

1. Substitution of the formula of the liquid water mixing ratio $q_w = \frac{4\pi\rho_w}{3\rho_a} N r^3$ into the equation for droplet radius evolution

$$r\frac{dr}{dt} = \frac{S}{F} \tag{B1}$$

leads to the equation for the decrease of q_w with the time

$$\frac{dq_w}{dt} = \frac{3}{F}\left(\frac{4\pi\rho_w}{3\rho_a}\right)^{2/3} N^{2/3} S q_w^{1/3} = B N^{2/3} S q_w^{1/3} \tag{B2}$$

where

$$B = \frac{3}{F}\left(\frac{4\pi\rho_w}{3\rho_a}\right)^{2/3} = \text{const} \tag{B3}$$

2. Equation for supersaturation is written as (Korolev and Mazin, 2003)

$$\frac{1}{S+1}\frac{dS}{dt} = -A_2\frac{dq_w}{dt} \tag{B4}$$

Integration of this equation under the assumption that $A_2 = \text{const}$ leads to the equation

$$\ln[S(t)+1] = -A_2 q_w(t) + C \tag{B5}$$

where C is determined by initial conditions at $t = 0$

$$C = \ln(S_0 + 1) + A_2 q_{w0} \tag{B6}$$

Using Eqs. (A5) and (A6) one obtains the equation with respect to $S(t)$

$$S(t) = (S_0 + 1)\exp\{-A_2[q_w(t) - q_{w0}]\} - 1 \tag{B7}$$

ACPD
15, 30269–30320, 2015

3. Mutual substitution of Eqs. (A2) and (A7) leads to the closed differential equations for $q_w(t)$ and $S(t)$

$$\frac{dq_w}{dt} = BN^{2/3}[(S_0+1)\exp\{-A_2(q_w - q_{w0})\} - 1]q_w^{1/3} \quad \text{(B8)}$$

$$\frac{1}{S+1}\frac{dS}{dt} = -A_2 BN^{2/3} S\left(q_{w0} - \frac{1}{A_2}\ln\frac{S+1}{S_0+1}\right)^{1/3} \quad \text{(B9)}$$

Equations (A8) and (A9) should be solved with initial conditions $q_w(0) = q_{w0}$ and $S(0) = S_0$ respectively.

4. In case $|S_0| \ll 1$, supersaturation is close to zero all the time $|S(t)| \ll 1$ and Eqs. (A7)–(A9) can be simplified as follows

$$S(t) = S_0 - A_2[q_w(t) - q_{w0}] \quad \text{(B10)}$$

$$\frac{dq_w}{dt} = -BN^{2/3}\left(A_2 q_w^{4/3} - (A_2 q_{w0} + S_0)q_w^{1/3}\right) \quad \text{(B11)}$$

$$\frac{dS}{dt} = -B(A_2 N)^{2/3}(A_2 q_{w0} + S_0 - S)^{1/3} S \quad \text{(B12)}$$

Then one can obtain Eqs. (A10)–(A12) in a non-dimensional form. Let us define time scale $\tau_0 = (BA_2 N^{2/3} q_w^{1/3})^{-1}$, normalized liquid water mixing ratio $\widetilde{q} = \frac{q}{q_{w0}}$, normalized supersaturation $\widetilde{S} = \frac{S}{A_2 q_{w0}}$, and non-dimensional time $\widetilde{t} = t/\tau_0 = BA_2 N^{2/3} q_{w0}^{1/3} t$. The Eqs. (A10)–(A12) can be rewritten in a non-dimensional form as

$$\widetilde{S}(\widetilde{t}) = -\widetilde{q}(\widetilde{t}) + \gamma \quad \text{(B13)}$$

$$\frac{d\widetilde{q}}{d\widetilde{t}} = \widetilde{q}^{1/3}(\gamma - \widetilde{q}) \quad \text{(B14)}$$

ACPD
15, 30269–30320, 2015

$$\frac{d\widetilde{S}}{d\widetilde{t}} = -(\gamma - \widetilde{S})^{1/3}\widetilde{S} \tag{B15}$$

where non-dimensional parameter $\gamma = 1 + \frac{S_0}{A_2 q_{w0}}$ depends on initial supersaturation S_0 and initial liquid water mixing ratio q_{w0}. Equation (A14) should be solved with initial condition $\widetilde{q}(0) = 1$ and Eq. (A15) should be solved with initial condition $\widetilde{S}(0) = \frac{S_0}{A_2 q_{w0}} < 0$. Note that Eqs. (A14) and (A15) are rigidly connected by Eq. (A13).

Acknowledgements. This research was supported by the Israel Science Foundation (grant 1393/14), the Office of Science (BER), US Department of Energy Award DE-SC0006788 and the Binational US-Israel Science foundation (grant 2010446). A. Korolev's participation was supported by Environment Canada.

References

Anthes, R. A.: Tropical Cyclones – Their Evolution, Structure, and Effects, Monograph 41, Amer. Meteorol. Soc., 208 pp., 1982.

Baker, M. and Latham, J.: The evolution of droplet spectra and the rate of production of embyonic raindrops in small cumulus clouds, J. Atmos. Sci., 36, 1612–1615, 1979.

Baker, M. B. and Latham, J.: A diffusive model of the turbulent mixing of dry and cloudy air, Q. J. Roy. Meteor. Soc., 108, 871–898, 1982.

Baker, M., Corbin, R. G., and Latham, J.: The influence of entrainment on the evolution of cloud drop spectra: I. A model of inhomogeneous mixing, Q. J. Roy. Meteor. Soc., 106, 581–598, 1980.

Bar-Or, R. Z., Koren, I., Altaratz, O., and Fredj, E.: Radiative properties of humidified aerosol in cloudy environment, Atmos. Res., 118, 280–294, 2012.

Benmoshe, N., Pinsky, M., Pokrovsky, A., and Khain, A.: Turbulent effects on the microphysics and initiation of warm rain in deep convective clouds: 2-D simulations by a spectral mixed-phase microphysics cloud model, J. Geophys. Res., 117, 1–20, 2012.

ACPD
15, 30269–30320, 2015

Blyth, A. M., Choularton, T. W., Fullarton, G., Latham, J., Mill, C. S., Smith, M. H., and Stromberg, I. M.: The Influence of entrainment on the evolution of cloud droplet spectra. 2. Field experiments 5 at Great Dun Fell, Q. J. Roy. Meteor. Soc., 106, 821–840, 1980.
Burnet, F. and Brenguier, J.-L.: Observational study of the entrainment-mixing process in warm convective clouds, J. Atmos. Sci., 64, 1995–2011, 2007.
Denvich, B. J., Bartello, P., Brenguier, J.-L., Collins, L. R., Grabowski, W. W., Ijzermans, R. H. A., Malinovski, S. P., Reeks, M. W., Vassilicos, J. C., Wang, L.-P., and Warhaft, Z.: Droplet growth in warm turbulent clouds, Q. J. Roy. Meteor. Soc., 138, 1401–1429, 2012.
De Rooy, W. C., Bechtold, P., Fröhlich, K., Hohenegger, C., Jonker, H., Mironov, D., Siebesma, A. P., Teixeira, J., and Yano, J.-I.: Entrainment and detrainment in cumulus convection: an overview, Q. J. Roy. Meteor. Soc., 139, 1–19, 2013.
Dimotakis, P. E.: Turbulent mixing, Annu. Rev. Fluid Mech., 37, 329–356, 2005.
Ferrier, B. S. and Houze, R. A.: One-dimensional time dependent modeling of GATE cumulonimbus convection, J. Atmos. Sci., 46, 330–352, 1989.
Gerber, H., Frick, G., Jensen, J. B., and Hudson, J. G.: Entrainment, mixing, and microphysics in trade-wind cumulus, J. Meteorol. Soc. Jpn., 86A, 87–106, 2008.
Ghan, S. J., Abdul-Razzak, H., Nenes, A., Ming, Y., Liu, X., Ovchinnikov, M., Shipway, B., Meskhidze, N., Xu, J., and Shi, X.: Droplet nucleation: physically-based parameterizations and comparative evaluation, J. Adv. Model. Earth Syst., 3, M10001, doi:10.1029/2011MS000074, 2011.
Goix, P. J. and Talbot, L.: Turbulent counter flow diffusion flame structure and dilution effects combustion, Sci. Technol., 79, 4–6, 1991.
Hill, A. A., Feingold, G., and Jiang, H.: The influence of entrainment and mixing assumption on aerosol–cloud interactions in marine stratocumulus, J. Atmos. Sci., 66, 1450–1464, 2009.
Kerstein, A. R.: Linear eddy modelling of turbulent scalar transport and mixing, Combust. Sci. Technol., 60, 391–421, 1988.
Kerstein, A. R.: Linear-eddy modelling of turbulent transport. Part 6. Microstructure of diffusive scalar mixing fields, J. Fluid Mech., 231, 361–394, 1991.
Khain, A., Prabha, T. V., Benmoshe, N., Pandithurai, G., and Ovchinnikov, M.: The mechanism of first raindrops formation in deep convective clouds, J. Geophys. Res.-Atmos., 118, 9123–9140, 2013.
Khain, A. P., Beheng, K. D., Heymsfield, A., Korolev, A., Krichak, S. O., Levin, Z., Pinsky, M., Phillips, V., Prabhakaran, T., Teller, A., van den Heever, S. C., and Yano, J.-I.: Representation

ACPD
15, 30269–30320, 2015

of microphysical processes in cloud-resolving models: spectral (bin) microphysics vs. bulk parameterization, Rev. Geophys., 53, 247–322, 2015.
Knight, C. A. and Miller, L. J.: Early radar echoes from small, warm cumulus: Bragg and hydrometeor scattering, J. Atmos. Sci., 55, 2974–2992, 1998.
Korn, G. A. and Korn, T. M.: Mathematical Handbook for Scientists and Engineers: Definitions, Theorems, and Formulas for Reference and Review, Courier Corporation – Mathematics, MGRAW-HILL Book Company, Inc. NY, Toronto, London, 712 pp., 2000.
Korolev, A. V.: The influence of suresaturation fluctuations on droplet size spectra formation, J. Atmos. Sci., 52, 3620–3634, 1995.
Korolev, A. V. and Isaac, G. A.: Drop growth due to high supersaturation caused by isobaric mixing, J. Atmos. Sci., 57, 1675–1685, 2000.
Korolev, A. V. and Isaac, G. A.: Phase transformation of mixed-phase clouds, Q. J. Roy. Meteor. Soc., 129, 19–38, 2003.
Korolev, A. V. and Mazin, I. P.: Supersaturation of water vapor in clouds, J. Atmos. Sci., 60, 2957–2974, 2003.
Korolev, A., Khain, A., Pinsky, M., and French, J.: Theoretical study of mixing in liquid clouds – Part 1: Classical concept, Atmos. Chem. Phys. Discuss., 15, 30211–30267, doi:10.5194/acpd-15-30211-2015, 2015.
Kumar, B., Schumacher, J., and Shaw, R. A.: Cloud microphysical effects of turbulent mixing and entrainment, Theor. Comput. Fluid Dyn., 27, 361–376, 2013.
Latham, J. and Reed, R. L.: Laboratory studies of effects of mixing on evolution of cloud droplet spectra, Q. J. Roy. Meteor. Soc., 103, 297–306, 1977.
Lehmann, K., Siebert, H., and Shaw, R. A.: Homogeneous and inhomogeneous mixing in cumulus clouds: dependence on local turbulence structure, J. Atmos. Sci., 66, 3641–3659, 2009.
Mazin, I. P.: Effect of phase transition on formation of temperature and humidity stratification in clouds, in: Proc. Int. Conf. on Cloud Physics, Toronto, Ontario, Canada, Amer. Meteor. Soc., 132–137, 1968.
Magaritz-Ronen, L., Pinsky, M., and Khain, A.: Effects of turbulent mixing on the structure and macroscopic properties of stratocumulus clouds demonstrated by a Lagrangian trajectory model, J. Atmos. Sci., 71, 1843–1862, 2014.
Monin, A. S. and Yaglom, A. M.: Statistical Fluid Mechanics: Mechanics of Turbulence, vol. 2, MIT Press, 911 pp., 1975.

ACPD
15, 30269–30320, 2015

Pinsky, M. and Khain, A. P.: Effects of in-cloud nucleation and turbulence on droplet spectrum formation in cumulus clouds, Q. J. Roy. Meteor. Soc., 128, 1–33, 2002.
Pinsky, M., Mazin, I. P., Korolev, A., and Khain, A.: Supersaturation and diffusional drop growth in liquid clouds, J. Atmos. Sci., 70, 2778–2793, 2013.
Pruppacher, H. R. and Klett, J. D.: Microphysics of clouds and precipitation, 2nd Edn., Oxford Press, 914 p., 1997
Stull, R. B.: An Introduction to Boundary Layer Meteorology, Springer, the Netherlands, 666 pp., 1988.
Troen, I. and Mahrt, L.: A simple model of the atmospheric boundary layer: sensitivity to surface evaporation, Bound.-Lay. Meteorol., 37, 129–148, 1986.
Warhaft, Z.: Passive scalars in turbulent flows, Annu. Rev. Fluid Mech., 32, 203–240, 2000.
Warner, J.: The microstructure of cumulus cloud. Part 1: General features of the droplet spectrum, J. Atmos. Sci., 26, 1049–1059, 1969.

ACPD
15, 30269–30320, 2015

Table 1. Linear scales of volumes experiencing homogeneous mixing under conditions typical of different cloud types.

Cloud type	N, cm^{-3}	q_w, $g\,m^{-3}$	r, µm	Dissipation rate, $cm^2\,s^{-3}$	Phase relaxation time, s	Phase scale, m
Maritime convective	100	2.0	16.8	300	2.01	0.49
Maritime Stratocumulus	100	0.5	10.6	10	3.19	0.18
Weak Stratocumulus	100	0.2	7.8	5	4.33	0.2
Continental convective	500	2	8.0	500	0.75	0.6

ACPD
15, 30269–30320, 2015

Table 2. Estimations of results of mixing under different environmental conditions*.

T (°C)	A_2	q_{w1}, g kg^{-1}	RH$_2$ %	μ (fraction of cloudy air)	$R\frac{1-\mu}{\mu}$	Result of mixing
$T = 0$°C	400	1.0	95	0.5	−0.125	cloudy
$T = 0$°C	400	1.0	50	0.5	−1.25	Non-cloudy
−10°C	700	2.0	95	0.5	−0.036	cloudy
−10°C	700	2.0	50	0.5	−0.36	cloudy
−20°C	1500	2.0	95	0.5	−0.017	cloudy
−20°C	1500	2.0	50	0.5	−0.17	cloudy
−20°C	1500	2.0	95	0.1	−0.153	cloudy
−20°C	1500	2.0	50	0.1	−1.53	Non-cloudy

* The values A_2 are estimated using Pinsky et al. (2013).

ACPD
15, 30269–30320, 2015

Table 3. Parameters of initial Gamma distributions.

DSD	N_0, cm^3	α	β, μm	Modal radius, μm	LWC, g m^{-3}
Narrow	264.2	101.0	0.1	10.0	0.587
Wide	71.0	4.3	3.1	10.0	0.587

ACPD
15, 30269–30320, 2015

Table A1. List of symbols.

Symbol	Description	Units
A_2	$\frac{1}{q_v} + \frac{L_e^2}{c_p R_v T^2}$, coefficient	–
B	$\frac{3}{F}\left(\frac{4\pi\rho_w}{3\rho_a}\right)^{2/3}$	$m^2\,s^{-1}$
C	constant of integration	–
c_p	specific heat capacity of moist air at constant pressure	$J\,kg^{-1}\,K^{-1}$
D	coefficient of water vapour diffusion in the air	$m^2\,s^{-1}$
e	water vapor pressure	$N\,m^{-2}$
e_w	saturation vapour pressure above flat surface of water	$N\,m^{-2}$
F	$\left(\frac{\rho_w L_e^2}{k_a R_v T^2} + \frac{\rho_w R_v T}{e_w(T)D}\right)$, coefficient	$m^{-2}\,s$
$f(r,t)$	droplet size distribution	m^{-4}
$f_0(r_0)$	initial droplet size distribution	m^{-4}
k_a	coefficient of air heat conductivity	$J\,m^{-1}\,s^{-1}\,K^{-1}$
L_{mix}	characteristic spatial scale of mixing	m
L_{pr}	spatial scale of phase relaxation	m
L_w	latent heat for liquid water	$J\,kg^{-1}$
N	droplet concentration	m^{-3}
N_1	droplet concentration in cloudy volume	m^{-3}
p	pressure of moist air	$N\,m^{-2}$
Q	change of square of droplet radius	m^2
r	droplet radius	m
R	$\frac{S_0}{A_2 q_{w1}}$, non-dimensional parameter	–
R_a	specific gas constant of moist air	$J\,kg^{-1}\,K^{-1}$
R_v	specific gas constant of water vapor	$J\,kg^{-1}\,K^{-1}$
q_v	water vapor mixing ratio (mass of water vapor per 1 kg of dry air)	–
q_w	liquid water mixing ratio (mass of liquid water per 1 kg of dry air)	–
q_{w0}	initial liquid water mixing ratio	–
q_{w1}	liquid water mixing ratio in cloudy volume	–
$\tilde{q}$	normalised liquid water mixing ratio	–
$\tilde{q}_{min}$	normalized equilibrium LWC	–
S	$e/e_w - 1$, supersaruration over water	–
S_0	initial supersaturation	–
S_2	supersaturation in dry volume	–
$\tilde{S}_{max}$	maximal normalized supersaturation	–
$\tilde{S}$	normalized supersaturation	–
T	temperature	K
t_e	normalized evaporation time	–
t	Time	s
$\tilde{t}$	non-dimensional time	–
$x(\tilde{r})$	non-dimensional variable	–
α	parameter of Gamma distribution	–
β	parameter of Gamma distribution	m^{-1}
χ	$\gamma^{1/3}$, non-dimensional parameter	–
ε	turbulent dissipation rate	$m^2\,s^{-3}$
γ	$1 + \frac{S_0}{A_2 q_{w0}}$, non-dimensional parameter	–
μ	mass fraction of cloudy air	–
ρ_a	density of the air	$kg\,m^{-3}$
ρ_w	density of liquid water	$kg\,m^{-3}$
τ_{pr}	phase relaxation time	s
τ_{mix}	characteristic time of mixing	s
τ_0	time scale	s

ACPD
15, 30269–30320, 2015

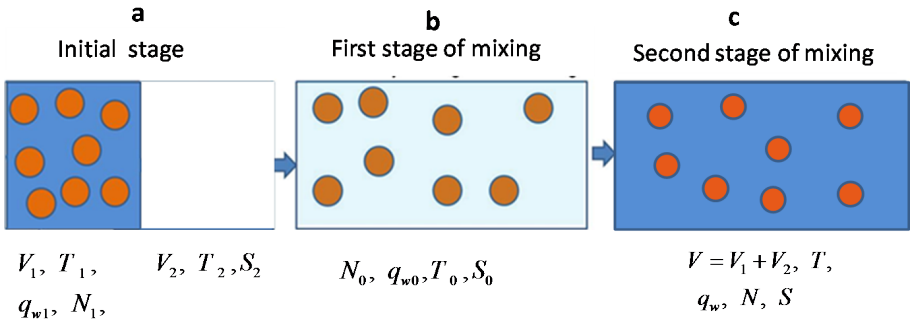

Figure 1. Conceptual scheme of homogeneous mixing in a case of monodisperse DSD. The subsaturated volume of dry air is denoted by white, the cloudy volumes with saturated air are denoted by dark blue. The volume forming as a result of the mixing process after total homogenization is marked by light blue. Index 1 shows initial values characterizing initially cloudy volume. Index 2 denotes initial values in non-cloudy volume. Index 0 denotes values in the total volume after the first stage of mixing.

ACPD
15, 30269–30320, 2015

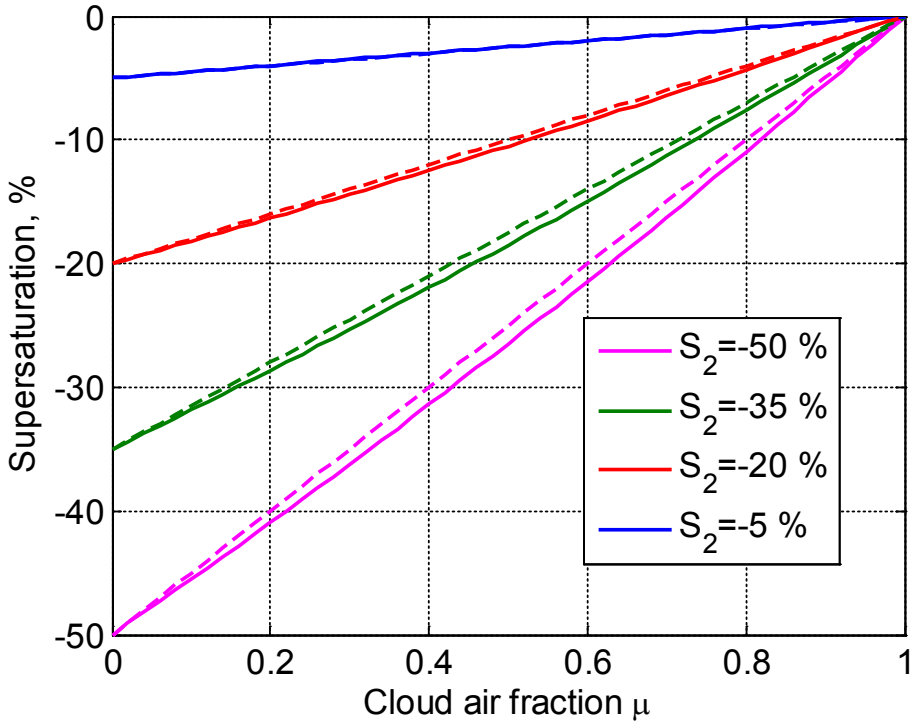

Figure 2. Dependence of resulting supersaturation on parameter μ (solid line) and approximate linear dependence calculated using Eq. (6b) (dashed line). Initial temperatures of two volumes are $T_1 = 8\,^{\circ}\mathrm{C}$ and $T_2 = 10\,^{\circ}\mathrm{C}$.

ACPD
15, 30269–30320, 2015

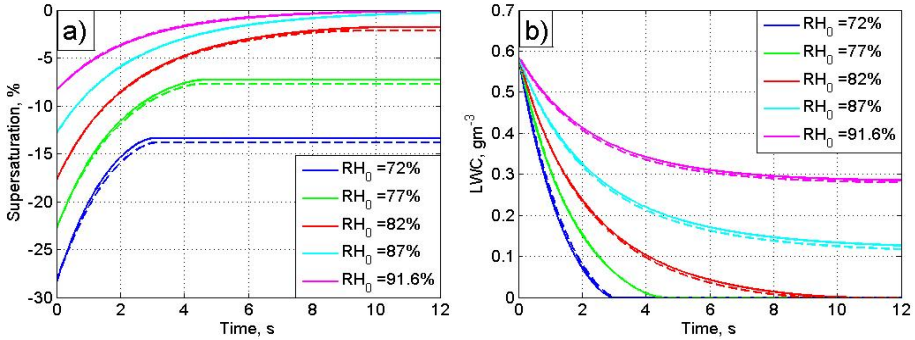

Figure 3. Dependencies $S(t)$ **(a)** and $q_w(t)$ **(b)**, calculated under different initial relative humidity RH_0 using closed differential Eqs. (12) and (13) (solid lines) and corresponding dependencies calculated using a parcel model (dashed lines). The parameters of the calculations are T_0 = 10 °C, p_0 = 842 mb, r_0 = 10 µm, N_0 = 140 cm^{-3}, q_{w0} = 0.29 g m^{-3}.

ACPD
15, 30269–30320, 2015

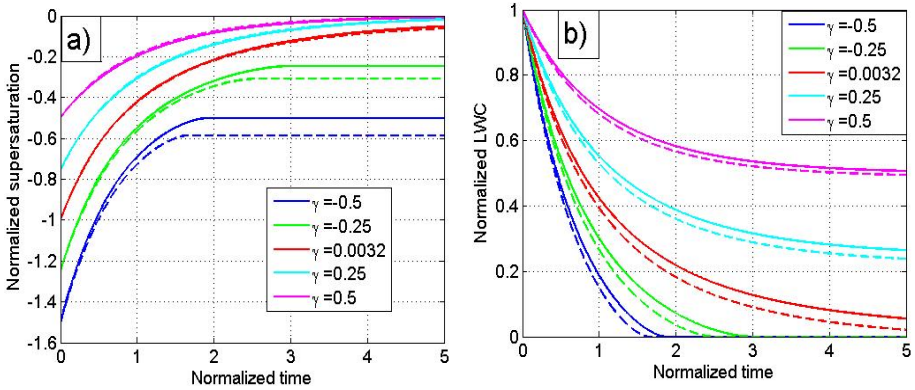

Figure 4. Universal dependencies $\widetilde{S}(\widetilde{t})$ **(a)** and $\widetilde{q}(\widetilde{t})$ **(b)**, calculated under different parameters γ using Eqs. (17) and (18) (solid lines) and corresponding dependencies, calculated using a parcel model (dashed lines).

ACPD
15, 30269–30320, 2015

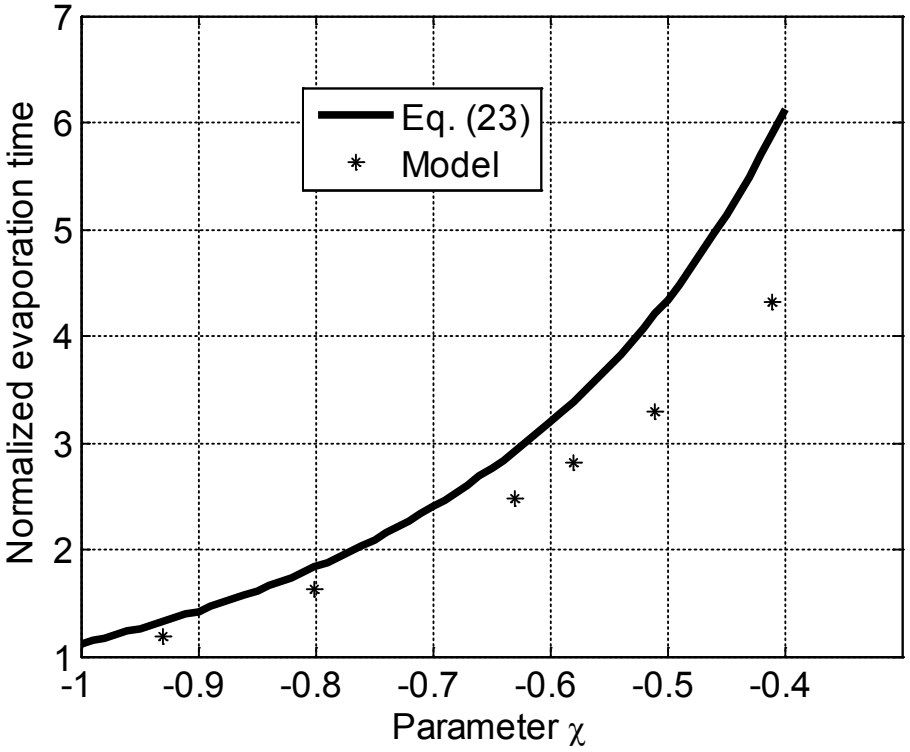

Figure 5. Dependence of evaporation time on parameter χ, $t_e(\chi)$. Time is measured in relaxation time scales. The values obtained using parcel model are shown by asterisks.

ACPD
15, 30269–30320, 2015

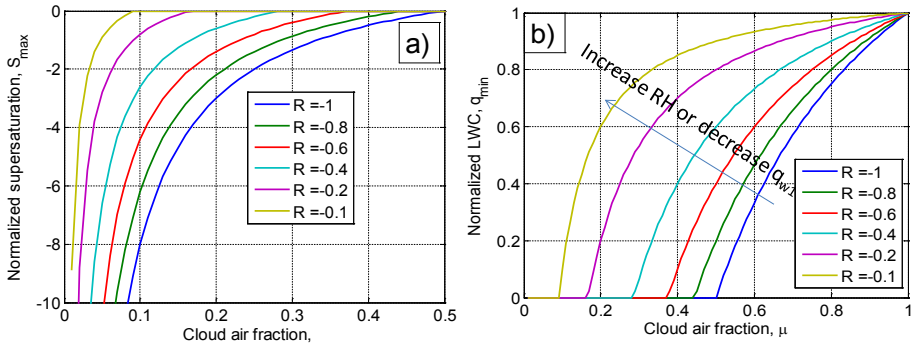

Figure 6. Dependencies of normalized supersaturation **(a)** and normalized LWC **(b)** on cloudy air fraction at the final stage of homogeneous mixing. Curves of different colors correspond to different values of non-dimensional parameter $R = \frac{S_2}{A_2 q_{w1}}$.

ACPD
15, 30269–30320, 2015

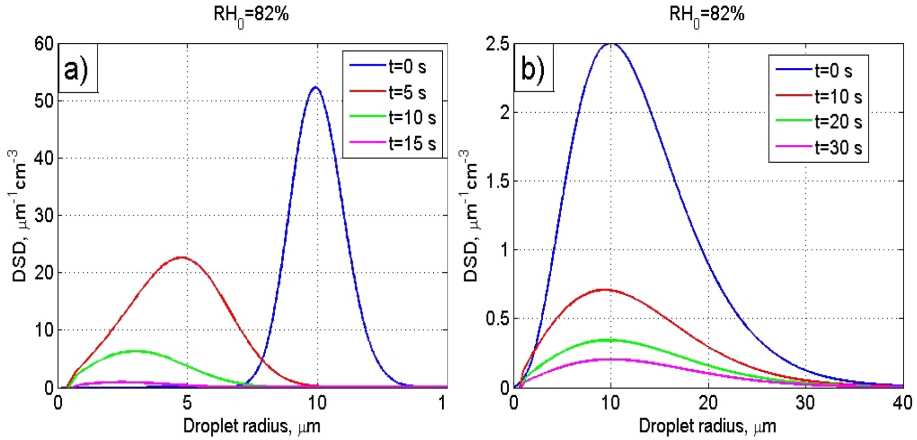

Figure 7. Time evolution of initially narrow DSD **(a)**, and initially wide DSD **(b)**. Initial parameters of calculation are the same for both examples: $T_0 = 10\,^{\circ}\mathrm{C}$, $p = 829\,\mathrm{mb}$, $\mathrm{RH}_0 = 82\,\%$, $q_{w0} = 0.587\,\mathrm{g\,m^{-3}}$. Parameters of initial Gamma distribution are given in Table 3.

ACPD
15, 30269–30320, 2015

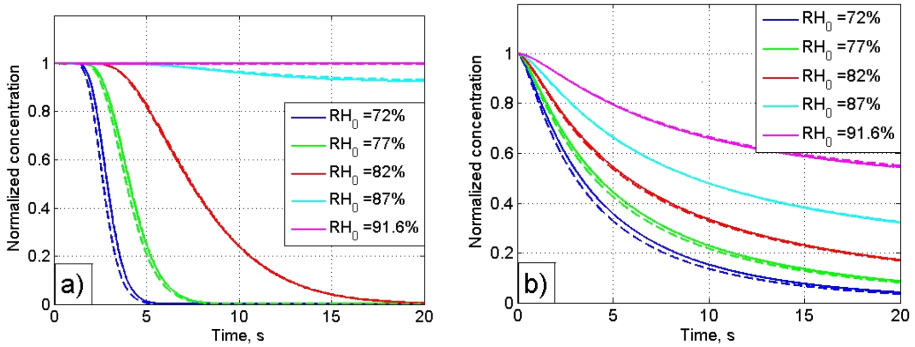

Figure 8. Time dependencies of normalized droplet concentration for initially narrow **(a)** and wide **(b)** DSDs under initially different RH_0 in the resulting volume. The dependencies are calculated directly using a parcel model (solid lines) and using Eq. (33) (dashed lines). The thermodynamic parameters are the same as in Fig. 7. Parameters of initial DSDs are given in Table 3.

ACPD
15, 30269–30320, 2015

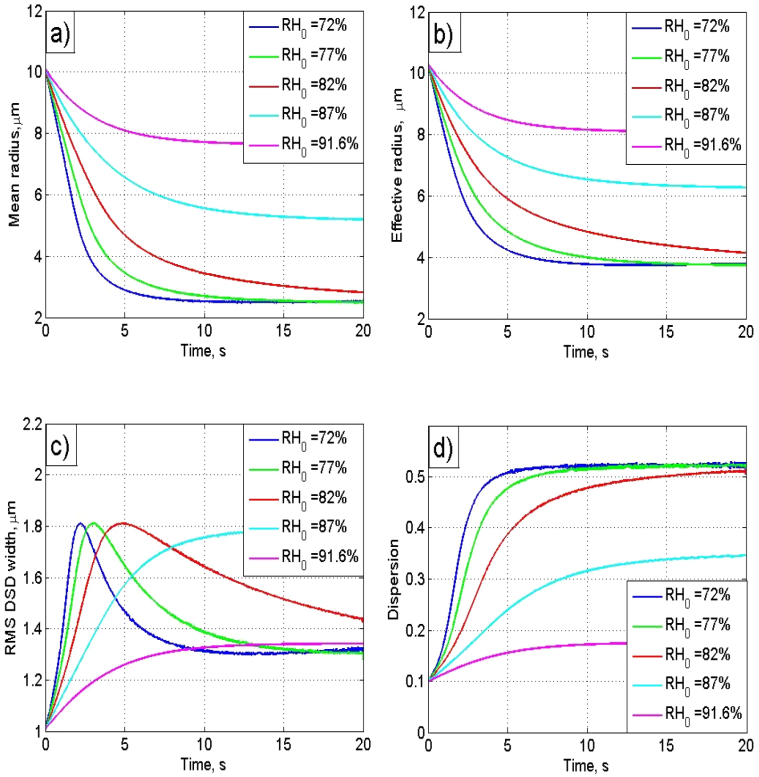

Figure 9. Dependencies of moment functions typically used for characterizing DSD shape under different initial relative humidity RH_0 in the resulting volume. The dependencies are calculated using a parcel model for an initially narrow DSD (see Table 3). The thermodynamic parameters are the same as in Fig. 7.

ACPD
15, 30269–30320, 2015

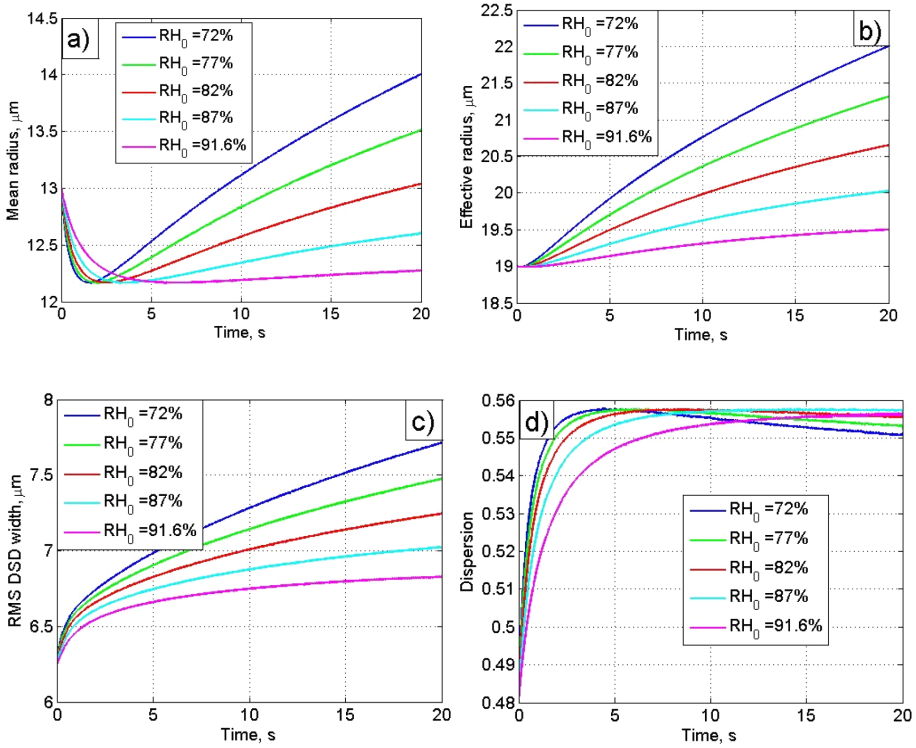

Figure 10. The same as in Fig. 9 but for an initially wide DSD.

ACPD
15, 30269–30320, 2015

Theoretical investigation of mixing in warm clouds – Part 2

M. Pinsky et al.

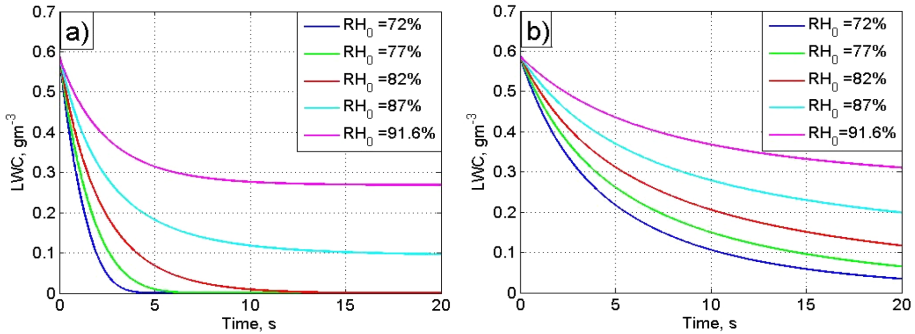

Figure 11. Time dependencies of LWC calculated under different RH_0 in the resulting volume. The dependencies are calculated using a parcel model for an initially narrow DSD **(a)** and an initially wide DSD **(b)**. The thermodynamic parameters are the same as in Fig. 7. The parameters of initial DSDs are given in Table 3.

ACPD
15, 30269–30320, 2015

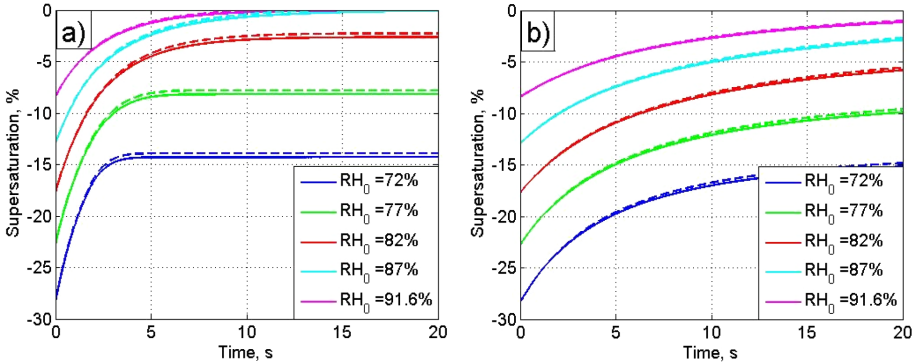

Figure 12. Time dependencies of supersaturation calculated under different initial relative humidity RH_0 in the resulting volume. The dependencies are calculated using Eq. (8) (solid lines) and Eq. (40) (dashed lines) for an initially narrow DSD **(a)** and an initially wide DSD **(b)**. The thermodynamic parameters are the same as in Fig. 7. The parameters of initial DSDs are given in Table 3.

ACPD
15, 30269–30320, 2015

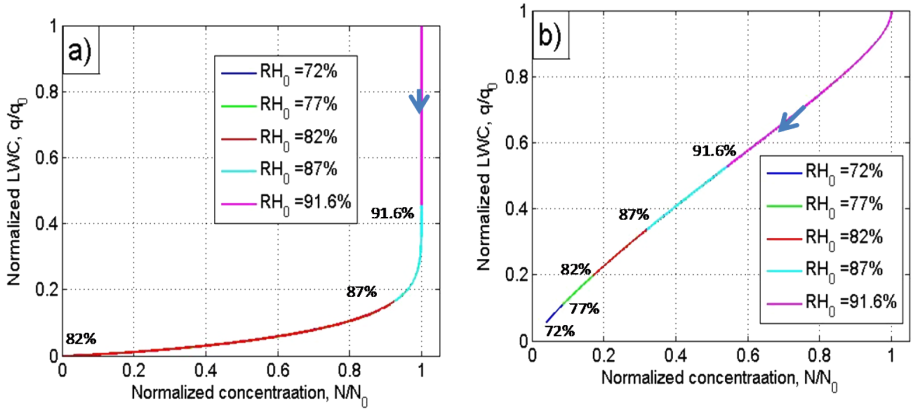

Figure 13. Dependencies of normalized LWC on the normalized number concentration of droplets calculated under different initial relative humidity RH_0 in the resulting volume. The dependencies are calculated for an initially narrow DSD **(a)** and an initially wide DSD **(b)**. The thermodynamic parameters are the same as in Fig. 7. The parameters of the initial DSDs are given in Table 3. Arrows denote the direction of increasing time.

ACPD
15, 30269–30320, 2015